

# Slip-Flow Pressure Drop in Microchannels of General Cross Section

**M. Bahrami**<sup>1</sup>

Assistant Professor  
e-mail: mbahrami@sfu.ca

**A. Tamayol**

Ph.D. Student  
e-mail: ata42@sfu.ca

Mechatronic Systems Engineering,  
School of Engineering Science,  
Simon Fraser University,  
BC, V3T 0A3, Canada

**P. Taheri**

Ph.D. Candidate  
Department of Mechanical Engineering,  
University of Victoria,  
P.O. Box 3055,  
Stn. CSC,  
Victoria, BC, V8W 3P6, Canada

*In the present study, a compact analytical model is developed to determine the pressure drop of fully-developed, incompressible, and constant properties slip-flow through arbitrary cross section microchannels. An averaged first-order Maxwell slip boundary condition is considered. Introducing a relative velocity, the difference between the bulk flow and the boundary velocities, the axial momentum reduces to Poisson's equation with homogeneous boundary condition. Square root of area is selected as the characteristic length scale. The model of Bahrami et al. (2006, "Pressure Drop of Laminar, Fully Developed Flow in Microchannels of Arbitrary Cross Section," ASME J. Fluids Eng., 128, pp. 1036–1044), which was developed for no-slip boundary condition, is extended to cover the slip-flow regime in this study. The proposed model for pressure drop is a function of geometrical parameters of the channel: cross sectional area, perimeter, polar moment of inertia, and the Knudsen number. The model is successfully validated against existing numerical and experimental data collected from different sources in literature for several shapes, including circular, rectangular, trapezoidal, and double-trapezoidal cross sections and a variety of gases such as nitrogen, argon, and helium.*

[DOI: 10.1115/1.3059699]

*Keywords:* slip-flow, microchannels, general cross section, pressure distribution

## 1 Introduction

The fast-paced growth of microfluidic systems and their applications in electronics cooling, aerospace, micro electro mechanical systems (MEMS), medical, and biomedical devices has motivated many researchers to investigate microscale transport phenomena [1–3]. Microchannels are essential components of many microfluidic devices [4]. Several factors that differentiate microscale from conventional flows have been identified through a number of experimental, numerical, and analytical studies. These factors include noncontinuum regimes, surface roughness, and compressibility effects [5–7]. Due to the small size of these channels, the length scale is comparable to molecular mean free path; thus, deviation from the continuum theory should be considered. The nondimensional parameter used for analyzing this deviation is the Knudsen number defined as

$$\text{Kn} = \frac{\lambda}{\mathcal{L}} \quad (1)$$

where  $\lambda$  is the molecular mean free path and  $\mathcal{L}$  is an appropriate length scale of the channel. When the Knudsen number is in the range of  $0.001 < \text{Kn} < 0.1$ , a nonequilibrium state occurs very close to the wall, which is initiated from domination of molecular collisions with the walls over intermolecular collisions [8]. Hence, no-slip boundary condition is no longer valid on channel boundaries, where a slip-velocity exists. However, for the rest of the flow, the continuum assumption still holds. This is called *slip-flow regime*.

Pressure drop in microconduits with different cross sections including noncontinuum effects has been the subject of several

investigations. In rarefied gas flow, the friction factor reduces as the Knudsen number increases. This is demonstrated theoretically by Pfahler et al. [9], Ebert and Sparrow [10], Harley et al. [11], Morini and Spiga [12], and Beskok and Karniadakis [13]. Experimental studies conducted by Harley et al. [11], Choi et al. [14], Yu et al. [15], Arkilic et al. [16,17], Araki et al. [18], and Kim et al. [4] confirm that the continuum assumption with no-slip velocity on walls is unable to predict the flow behavior in microchannels in this range of Knudsen number.

Pfahler et al. [9] performed one of the first analytical and experimental investigations on rarefied flows. They reported the existence of slip-flow in microchannels through measuring an increase in mass flow rate when compared with the predicted values from the continuum (no-slip) theory.

Kim et al. [4] reported experimental data for rarefied flow through microtubes over the range of  $0.0008 < \text{Kn} < 0.09$  and  $0.03 < \text{Re} < 30$ . They tested several gases such as nitrogen, helium, and argon. Araki et al. [18] reported results for pressure drop in trapezoidal and triangular channels in slip-flow regime where  $0.011 < \text{Kn} < 0.035$  and  $0.05 < \text{Re} < 4.2$  range. Arkilic et al. [16] included compressibility effects in their tests by conducting experiments in relatively higher Mach numbers. They also proposed an analytical model for analyzing compressible slip-flow in trapezoidal silicon microchannels; they did not report the range of Mach number in their tests. Arkilic et al. [17] conducted experiments to determine the effects of tangential momentum accommodation on the mass flow rate through trapezoidal microchannels in the slip-flow regime.

Ebert and Sparrow [9] formulated an analytical solution for slip-flow through rectangular channels. They realized that the effect of slip is to flatten the velocity distribution relative to that of a continuum flow. Assuming first-order slip boundary condition, Morini and co-workers [12,19] performed numerical studies for determination of pressure drop through microchannels of rectangular, circular, trapezoidal, and double-trapezoidal cross sections and reported their results in a tabular form for a range of cross section aspect ratio for the slip-flow regime. Using similar boundary conditions Khan and Yovanovich [20] developed a solution for

<sup>1</sup>Corresponding author.

Contributed by the Fluids Engineering Division of ASME for publication in the JOURNAL OF FLUIDS ENGINEERING. Manuscript received April 9, 2008; final manuscript received October 2, 2008; published online February 5, 2009. Assoc. Editor: Ali Beskok. Paper presented at the Sixth International Conference on Nanochannels, Microchannels and Minichannels (ICNMM2008), Darmstadt, Germany, June 23–30, 2008.

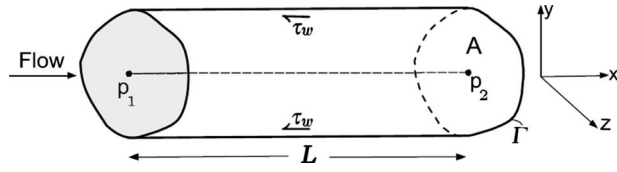


Fig. 1 Flow in arbitrary cross section microchannel

fluid flow and convective heat transfer in rectangular microchannels in slip-flow regime. Duan and Muzychka [21] proposed a model for the pressure drop of slip-flow through noncircular microchannels using the solution of the rectangular duct. They compared their model with the numerical data of Morini et al. [19] for common geometries. Their model is a function of the cross section aspect ratio defined for each geometry.

As a result of recent advances in microfabrication techniques, microchannels with different cross sectional geometries are fabricated for both commercial and scientific purposes. Bahrami et al. [22,23] developed a general model for prediction of pressure drop in microchannels of arbitrary cross section. Using the analytical solution of elliptical duct and the concept of Saint-Venant principle in torsion, they showed that the Poiseuille number,  $f Re$  [24], is a function of the polar moment of inertia, area, and perimeter of the cross section of the channel. Their model showed good agreement with experimental and numerical data for a wide variety of cross sections such as rectangular, trapezoidal, triangular, circular, and moon shaped. The model of Bahrami et al., however, is restricted to no-slip velocity regime. The objective of this paper is to extend the model of Bahrami et al. [22,23] to the slip-flow regime.

In this study, a general model is developed for predicting the Poiseuille number of fully-developed flow in arbitrary cross section microchannels with slip regime. The proposed model is validated with numerical and experimental data from different sources for a variety of geometries, including circular, rectangular, trapezoidal, and double-trapezoidal cross sections and several gases such as nitrogen, argon, and helium.

## 2 Problem Statement

Fully-developed laminar, constant properties, and incompressible flow in microchannels of constant general cross section is considered (Fig. 1). The Mach number,  $Ma = u/C$ , where  $C$  is the sound velocity, can be used to determine the importance of the compressibility effects [24]. In general, the compressibility effects can be neglected for the Mach numbers lower than 0.3 [24]. Due to the small size of microchannels, the average velocity is typically higher than conventional pipes. Consequently, the pressure drop and the Mach number are high in microchannels even in low Reynolds numbers. Morini et al. [19] argued that the Mach number is proportional to multiplication of the Knudsen and the Reynolds numbers. It should be noted that in spite of the negligible compressibility effects in a wide range of Reynolds number in low Knudsen numbers, these effects can be neglected only for very low Reynolds numbers at higher Knudsen numbers [19].

Based on the Knudsen number, flow regimes can be categorized into four groups: continuum (no-slip), slip-flow, transition, and molecular flows [25]. For slip-flow regime where  $0.001 < Kn < 0.1$ , errors due to the use of Navier–Stokes (NS) equations are negligible. However, no-slip boundary condition is no longer valid on walls and a slip-velocity should be considered [8]. The first-order Maxwell boundary condition for slip-velocity is

$$u_s = \frac{\sigma - 2}{\sigma} \lambda \left. \frac{\partial u}{\partial n} \right|_{\text{wall}} \quad (2)$$

where the thermal creep effects on the solid-fluid interface are neglected [25]. Here,  $u_s$  is the local slip-velocity,  $\sigma$  is the tangential momentum accommodation factor, which is considered unity

for most of engineering applications [26],  $\lambda$  is the molecular mean free path, and  $n$  is the normal vector to the wall. Using above-mentioned assumptions, the momentum equation reduces to

$$\frac{dP}{dx} = \mu \left( \frac{\partial^2 u}{\partial y^2} + \frac{\partial^2 u}{\partial z^2} \right) \quad (3)$$

This equation should be solved along with the following boundary condition:

$$u_s = \frac{\sigma - 2}{\sigma} \lambda \frac{\tau_w}{\mu}, \quad \tau_w = \mu \left. \frac{\partial u}{\partial n} \right|_{\text{wall}} \quad (4)$$

where  $\tau_w$  is the local wall shear stress. The set of governing equation and the boundary condition form a Poisson's equation with slip boundary condition. Because of the geometrical complexities, finding analytical solutions for the general cross section channels is highly unlikely. Therefore, we seek an approximate solution that can predict the pressure drop in arbitrary cross section with reasonable accuracy. This will provide a powerful tool that can be used in many practical instances such as basic design, parametric study, and optimization analyses, where often the trends and a reasonable estimate of the pressure drop are required.

## 3 Characteristic Length Scale

Selecting an appropriate and consistent characteristic length scale is an important part of developing a comprehensive general model. Selection of the characteristic length is an arbitrary choice and will not affect the final solution. However, a more appropriate length scale leads to more consistent results, especially when general cross section is considered. A circular duct is fully described with its diameter; thus the obvious length scale is the diameter (or radius). For noncircular cross sections, the selection is not as clear; many textbooks and researchers have conventionally chosen the hydraulic diameter,  $D_h$ , as the characteristic length. Yovanovich [27,28] introduced the square root of area ( $\sqrt{A}$ ) as a characteristic length scale for heat conduction and convection problems. Later, Muzychka and Yovanovich [29] proposed the use of  $\sqrt{A}$  for the fully-developed flow in noncircular ducts. Bahrami et al. [22,23] showed through analysis that  $\sqrt{A}$  appears in the solution of fully-developed flow in noncircular ducts. They also compared both  $D_h$  and  $\sqrt{A}$  and observed that using  $\sqrt{A}$  as the characteristic length scale results in similar trends in Poiseuille number for microchannels with a wide variety of cross sections. Therefore, in this study,  $\sqrt{A}$  is selected consistently as the length scale throughout the analysis and in the definition of the Knudsen number. Using  $\sqrt{A}$ , Eq. (4) becomes

$$u_s = \frac{\sigma - 2}{\sigma} Kn \sqrt{A} \frac{\tau_w}{\mu} \quad (5)$$

## 4 Model Development

Equation (5) shows that slip-velocity is related to local wall shear stress, which depends on the topology of the boundary and the cross section. Averaging the wall shear stress over the perimeter of the channel, Eq. (5) becomes [24]

$$\bar{u}_s = \frac{\sigma - 2}{\sigma} Kn \sqrt{A} \frac{\bar{\tau}_w}{\mu} \quad (6)$$

where  $\bar{u}_s$  and  $\bar{\tau}_w$  are the averaged slip-velocity and wall shear stress, respectively. Using an average (and constant) slip-velocity will simplify the solution to Eq. (3). This allows us to introduce a relative axial velocity,  $U$ , which is the difference between the bulk and the slip-velocities:

$$U = u - \bar{u}_s \quad (7)$$

After change in variable, Eq. (3) becomes

$$\frac{dP}{dx} = \mu \left( \frac{\partial^2 U}{\partial y^2} + \frac{\partial^2 U}{\partial z^2} \right) \quad (8)$$

Based on its definition, the relative velocity is zero on the channel walls. As a result, Eq. (8) becomes Poisson's equation with zero boundary condition. It is the same governing equation for fully-developed flow in the continuum regime. This equation has been solved for various geometries such as circular, rectangular, and elliptical ducts. The analytical solutions can be found in textbooks such as White [24] and Bejan [30]. A compact model for determination of Poiseuille number in general cross section channels has been presented by Bahrami et al. [22,23].

To determine the Poiseuille number,  $f$  Re, Bahrami et al. [22,23] used the analytical solution of Eq. (8) for elliptical channel. They presented the final result in the following easy-to-use form:

$$f \text{ Re}_{\sqrt{A}} = 32\pi^2 I_p^* \frac{\sqrt{A}}{\Gamma}, \quad I_p^* = \frac{I_p}{A^2} \quad (9)$$

$$\text{Re}_{\sqrt{A}} = \frac{\rho \bar{u} \sqrt{A}}{\mu}, \quad f = \frac{2\bar{\tau}_w}{\rho \bar{u}^2}$$

where  $I_p^*$  is the nondimensional polar moment of inertia of the cross section and  $f$  and  $\text{Re}_{\sqrt{A}}$  are the Fanning friction factor and Reynolds number based on  $\sqrt{A}$ , respectively. The elliptical channel was considered not because it is likely to occur in practice but rather to utilize the unique geometrical property of its velocity solution. The same approach is followed here. Starting from the elliptical cross section and using the axial relative velocity, one can find the average relative axial velocity  $\bar{U}$  for elliptical channels [24]:

$$\bar{U} = \frac{b^2 c^2}{4(b^2 + c^2)} \frac{\Delta P}{\mu L} \quad (10)$$

Applying a force balance in the channel leads to (see Fig. 1)

$$\bar{\tau}_w \Gamma L = \Delta P A \quad (11)$$

Cross sectional area and perimeter for elliptical channel are

$$A = \pi bc$$

$$\Gamma = 4bE(\sqrt{1 - \varepsilon^2}) \quad (12)$$

where  $E(\varepsilon) = \int_0^{\pi/2} \sqrt{1 - \varepsilon^2 \sin^2 x} dx$  is the complete elliptic integral of the second kind. Using Eqs. (11) and (12) and defining an aspect ratio,  $\varepsilon$ , as the ratio of the channel major and minor axes, the average velocity can be presented as [22]

$$\bar{U} = \frac{\sqrt{\varepsilon} E(\sqrt{1 - \varepsilon^2}) \bar{\tau}_w \sqrt{A}}{\sqrt{\pi^3} (1 - \varepsilon^2) \mu} \quad (13)$$

This equation can be rewritten as

$$\bar{U} = \frac{\Gamma \bar{\tau}_w}{16\pi^2 \mu I_p^*} \quad (14)$$

Using Eqs. (14) and (7), the average channel velocity,  $\bar{u}$ , becomes

$$\bar{u} = \frac{\Gamma \bar{\tau}_w}{16\pi^2 \mu I_p^*} + \frac{\sigma - 2}{\sigma} \text{Kn} \frac{\bar{\tau}_w \sqrt{A}}{\mu} \quad (15)$$

Introducing Fanning friction factor and after some simplifications, one can write

$$f \text{ Re}_{\sqrt{A}} = \frac{2}{\frac{\Gamma}{16\pi^2 \sqrt{A} I_p^*} + \frac{\sigma - 2}{\sigma} \text{Kn}} \quad (16)$$

Note that Eq. (16) is a general equation; in the continuum limit, where  $\text{Kn} \rightarrow 0$ , Eq. (16) yields the model of Bahrami et al. [22],

i.e., Eq. (9). The relationship between  $f$  Re for slip-flow regime and the continuum flow is

$$f \text{ Re}_{\sqrt{A}} = \frac{1}{\frac{1}{f \text{ Re}_{\sqrt{A}}^{\text{no-slip}}} + \frac{\sigma - 2}{2\sigma} \text{Kn}} \quad (17)$$

Following Morini et al. [19], reduction in friction coefficient in slip condition,  $\Phi$ , can be found as

$$\Phi = \frac{f \text{ Re}_{\sqrt{A}}}{f \text{ Re}_{\sqrt{A}}^{\text{no-slip}}} = \frac{1}{1 + \frac{\sigma - 2}{2\sigma} \alpha \text{Kn}} \quad (18)$$

where  $\alpha$  was determined through numerical analysis for each geometry in Ref. [19]. Using the present model, Eq. (16),  $\Phi$  can be found from

$$\Phi = \frac{f \text{ Re}_{\sqrt{A}}}{f \text{ Re}_{\sqrt{A}}^{\text{no-slip}}} = \frac{1}{1 + \frac{\sigma - 2}{\sigma} \frac{f \text{ Re}_{\sqrt{A}}^{\text{no-slip}}}{2} \text{Kn}} \quad (19)$$

Therefore,  $\Phi$  can be determined once  $f \text{ Re}_{\sqrt{A}}$  is known for the no-slip condition. Note that the value of  $\Phi$  is always equal to or less than unity.

## 5 Model Verification

Although the presented approach is based on analytical solution for elliptical cross section, the final relationship is a function of general geometrical parameters that can be calculated for any cross sections. In this section, the present model is compared with the numerical and the experimental data available for several common cross sections. The proposed model is verified with numerical results of Morini et al. [19] for circular, rectangular, trapezoidal, and double-trapezoidal microchannels as well as experimental data published by Kim et al. [4] and Araki et al. [18] for circular and trapezoidal ducts, respectively. For convenience, the geometrical parameters needed for different cross sections are listed in Table 1. In Secs. 5.1–5.4 the value of tangential momentum accommodation factor,  $\sigma$ , is assumed to be 1. The available data in literature were reported based on the hydraulic diameter. The Knudsen and the Poiseuille numbers based on the hydraulic diameter can be converted to  $\sqrt{A}$  basis using the following relationships:

$$f \text{ Re}_{\sqrt{A}} = f \text{ Re}_{D_h} \frac{\Gamma}{4\sqrt{A}} \quad (20)$$

$$\text{Kn}_{\sqrt{A}} = \text{Kn}_{D_h} \frac{4\sqrt{A}}{\Gamma}$$

**5.1 Circular Microchannels.** Using the geometrical parameters of circular channels listed in Table 1,  $f \text{ Re}_{\sqrt{A}}$  can be determined as

$$f \text{ Re}_{\sqrt{A}} = \frac{1}{\frac{1}{14.18} + \text{Kn}}, \quad \sigma = 1 \quad (21)$$

Morini et al. [19] proposed a similar correlation for  $f \text{ Re}_{\sqrt{A}}$ :

$$f \text{ Re}_{\sqrt{A}} = \frac{f \text{ Re}_{\sqrt{A}}^{\text{no-slip}}}{1 + 8 \text{Kn}} \quad (22)$$

In Table 2 the present model is compared with the analytical model proposed by Morini et al. [19], i.e., Eq. (22). As can be seen, the present model yields the exact same values reported in Ref. [19] over the slip-flow range of the Knudsen number.

**Table 1 Geometrical characteristics of different cross sections**

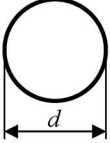

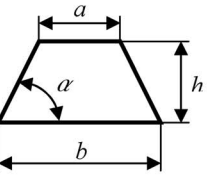
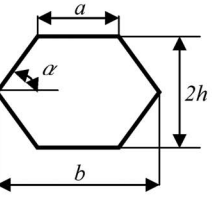
Cross-Section	Area ( $A$ )	Perimeter ( $\Gamma$ )	Non-Dimensional Polar Moment of Inertia ( $I_p^*$ )	Aspect Ratio ( $\varepsilon$ )
	$\frac{\pi d^2}{4}$	$\pi d$	$\frac{1}{2\pi}$	1
	$4ab$	$4(a+b)$	$\frac{1+\varepsilon^2}{12\varepsilon}$	$\frac{a}{b}$
	$\varepsilon h^2$	$2h\left(\varepsilon + \sqrt{\varepsilon^2 - \beta\varepsilon^2 + 1}\right)$	$\frac{(6\varepsilon^2 + 2) + \beta(1 - 3\varepsilon^2)}{36\varepsilon}$	$\frac{a+b}{2h}$
	$2\varepsilon h^2$	$2h\left[\left(2\sqrt{\varepsilon^2 - \beta\varepsilon^2 + 1}\right) + \varepsilon + \frac{1}{\tan\alpha}\right]$	$\frac{(6\varepsilon^2 + 2) + \beta(1 - 3\varepsilon^2)}{18\varepsilon} - \frac{8}{9\varepsilon}\left(3 - \frac{1}{\varepsilon \tan\alpha}\right)^2$	$\frac{a+b}{2h}$

Figure 2 shows the comparison between the present model and experimental data published by Kim et al. [4]. They conducted tests with nitrogen, argon, and helium over a range of  $0.0008 < Kn < 0.09$  and  $0.03 < Re < 30$ . The microtubes used in their experiments were made of quartz glass and had diameters ranging from  $5 \mu\text{m}$  to  $100 \mu\text{m}$ . According to Morini et al. [31] the experimental uncertainty of pressure drop measurements is on the order of 8–14%.

As can be seen, the present model captures the trends of the experimental data over a range of geometrical and thermophysical parameters. Also note that most of the data fall within the  $\pm 10\%$  bounds of the model.

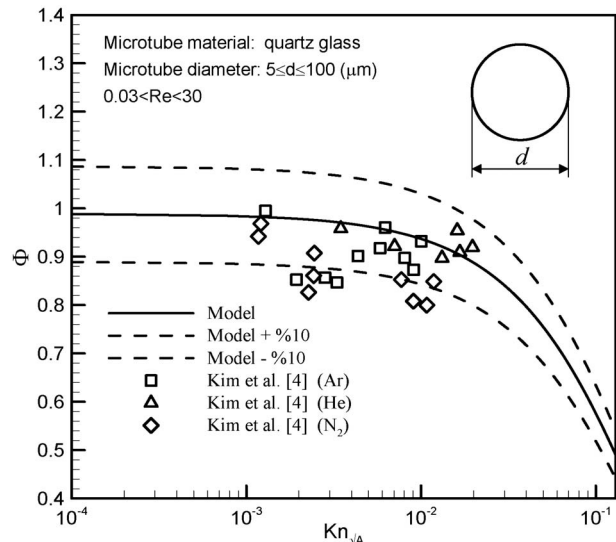
**5.2 Rectangular Microchannels.** The geometrical characteristics and schematic of rectangular channels are presented in Table 1. Substituting required parameters in Eq. (16),  $f Re_{\sqrt{A}}$  is determined as

**Table 2 Comparison between present model and analytical model of Morini et al. [19]**

Kn	$f Re_{\sqrt{A}}$ (model)	$f Re_{\sqrt{A}}$ [19]	$\Phi$
0	14.180	14.180	1.000
0.001	14.080	14.080	0.993
0.005	13.695	13.695	0.966
0.01	13.241	13.241	0.934
0.03	11.693	11.693	0.825
0.06	9.948	9.948	0.702
0.09	8.656	8.656	0.610
0.1	8.297	8.297	0.585

$$f Re_{\sqrt{A}}^{\text{slip}} = \frac{1}{\frac{1}{\frac{4\pi^2(1+\varepsilon^2)}{3\sqrt{\varepsilon}(1+\varepsilon)}} - Kn}, \quad \sigma = 1 \quad (23)$$

Table 3 and Fig. 3 show the comparison of the proposed model, Eq. (16), with numerical results of Morini et al. [19] for a range of



**Fig. 2 Comparison of the model with experimental data of Kim et al. [4] for circular channels**

**Table 3 Comparison between model and numerical data [19]; rectangular cross section**

$\varepsilon=0.01$				$\varepsilon=0.1$				$\varepsilon=0.3$			
Kn	$f Re_{\sqrt{A}}$ [19]	$f Re_{\sqrt{A}}$ (model)	Error (%)	Kn	$f Re_{\sqrt{A}}$ [19]	$f Re_{\sqrt{A}}$ (model)	Error (%)	Kn	$f Re_{\sqrt{A}}$ [19]	$f Re_{\sqrt{A}}$ (model)	Error (%)
0.0000	119.6	130.3	8.2	0.0000	36.8	38.2	3.6	0.0000	20.8	20.1	3.2
0.0002	118.2	128.6	8.2	0.0006	36.4	37.8	3.6	0.0008	20.6	20.0	3.1
0.0010	112.8	122.4	7.8	0.0029	34.9	36.2	3.7	0.0042	19.8	19.3	2.7
0.0015	109.8	118.8	7.6	0.0043	34.0	35.3	3.7	0.0063	19.4	18.9	2.4
0.0020	106.8	115.4	7.4	0.0057	33.2	34.4	3.7	0.0084	19.0	18.6	2.2
0.0050	92.1	98.5	6.5	0.0144	28.9	30.0	3.7	0.0211	16.8	16.6	1.0
0.0099	74.9	79.2	5.4	0.0287	23.7	24.7	3.7	0.0421	14.1	14.1	0.4
0.0149	63.1	66.2	4.7	0.0431	20.2	20.9	3.7	0.0632	12.1	12.3	1.5
0.0198	54.5	56.9	4.1	0.0575	17.5	18.2	3.8	0.0843	10.7	10.9	2.2

$\varepsilon=0.6$				$\varepsilon=0.8$				$\varepsilon=1$			
Kn	$f Re_{\sqrt{A}}$ [19]	$f Re_{\sqrt{A}}$ (model)	Error (%)	Kn	$f Re_{\sqrt{A}}$ [19]	$f Re_{\sqrt{A}}$ (model)	Error (%)	Kn	$f Re_{\sqrt{A}}$ [19]	$f Re_{\sqrt{A}}$ (model)	Error (%)
0.0000	15.5	14.4	7.1	0.0000	14.5	13.4	7.9	0.0000	14.2	13.2	8.1
0.0010	15.3	14.3	7.0	0.0010	14.4	13.3	7.8	0.0010	14.1	13.1	8.0
0.0048	14.9	14.0	6.5	0.0050	13.9	13.0	7.3	0.0050	13.7	12.7	7.4
0.0073	14.6	13.7	6.2	0.0075	13.7	12.8	7.0	0.0075	13.4	12.5	7.1
0.0097	14.3	13.5	5.9	0.0099	13.4	12.6	6.7	0.0100	13.2	12.3	6.8
0.0242	12.8	12.3	4.3	0.0248	12.1	11.5	5.1	0.0250	11.9	11.3	5.2
0.0484	10.9	10.7	2.3	0.0497	10.4	10.1	3.1	0.0500	10.2	9.9	3.1
0.0726	9.6	9.5	0.8	0.0745	9.1	8.9	1.6	0.0750	8.9	8.8	1.5
0.0968	8.5	8.5	0.3	0.0994	8.1	8.0	0.4	0.1000	8.0	7.9	0.3

$$\text{Error} = \frac{f Re_{\sqrt{A}} [19] - f Re_{\sqrt{A}} [\text{model}]}{f Re_{\sqrt{A}} [\text{model}]} \times 100$$

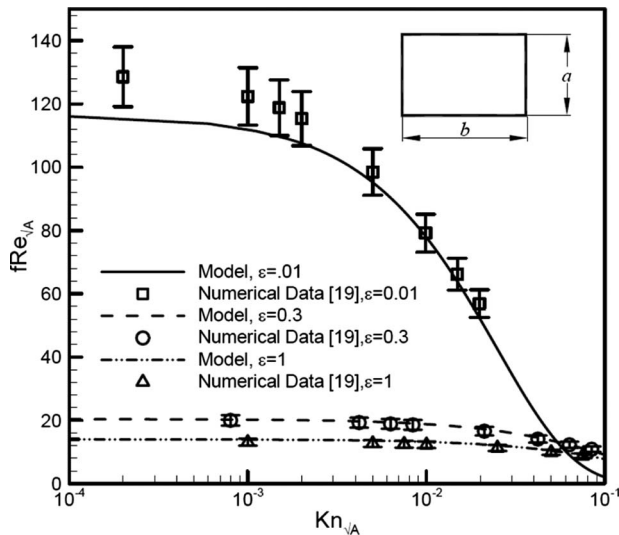
aspect ratio,  $0.01 \leq \varepsilon \leq 1$ . As can be seen, except for a few points, the agreement between the model and the numerical values is less than 8%.

**5.3 Trapezoidal Microchannels.** The cross section of an isosceles trapezoidal microchannel and its geometrical parameters are presented in Table 1. This is an important shape since this cross section is formed as a result of etching process in silicon wafers [19]. Furthermore, in the limit when the top side length,  $a$ , goes to zero, it yields an isosceles triangle and in another limit

when  $a=b$ , a rectangular channel will be formed. The geometrical characteristics of these limiting cases are listed in Table 4, where  $\beta$  in Tables 1 and 4 is a nondimensional parameter defined as

$$\beta = \frac{4ab}{(a+b)^2} \quad (24)$$

$\beta$  is zero for triangular and 1 for rectangular conduits. The angle  $\alpha$  (as shown in Table 1) is related to  $\beta$  and  $\varepsilon$  as [22]



**Fig. 3 Comparison of the model with numerical results of Morini et al. [19] for rectangular channels**

**Table 4 Limiting cases of isosceles trapezoid**

Cross section	$\varepsilon$	$\beta$	$f_p^*$	$\sqrt{A}/\Gamma$
Isosceles triangular	$\frac{b}{2h}$	0	$\frac{3\varepsilon^2 + 1}{18\varepsilon}$	$\frac{\sqrt{\varepsilon}}{2(\sqrt{\varepsilon^2 + 1} + \varepsilon)}$
Equilateral triangular	$\frac{1}{\sqrt{3}}$	0	$\frac{\sqrt{3}}{9}$	$\frac{\sqrt{3}}{6\sqrt{3}}$
Rectangular	$\frac{b}{h}$	1	$\frac{\varepsilon^2 + 1}{12\varepsilon}$	$\frac{\sqrt{3}}{2(1 + \varepsilon)}$
Square	1	1	$\frac{1}{6}$	$\frac{1}{4}$

**Table 5 Model versus data [19]; trapezoidal channels**

$\varepsilon=20.07$				$\varepsilon=5.07$				$\varepsilon=2.7$			
Kn	$f Re_{\sqrt{A}}$ [19]	$f Re_{\sqrt{A}}$ (model)	Error (%)	Kn	$f Re_{\sqrt{A}}$ [19]	$f Re_{\sqrt{A}}$ (model)	Error (%)	Kn	$f Re_{\sqrt{A}}$ [19]	$f Re_{\sqrt{A}}$ (model)	Error (%)
0.0000	53.4	56.6	5.6	0.0000	27.1	27.1	0.0	0.0000	18.6	17.9	3.8
0.0004	52.8	56.0	5.6	0.0007	26.8	26.8	0.1	0.0008	18.4	17.8	3.7
0.0021	50.5	53.5	5.5	0.0034	25.7	25.9	0.4	0.0042	17.8	17.3	3.2
0.0031	49.2	52.0	5.4	0.0052	25.1	25.3	0.6	0.0063	17.4	17.0	2.9
0.0041	48.0	50.7	5.4	0.0069	24.6	24.8	0.8	0.0084	17.1	16.7	2.6
0.0104	41.6	43.8	5.0	0.0172	21.6	21.9	1.7	0.0209	15.2	15.1	1.0
0.0207	34.0	35.7	4.7	0.0345	17.9	18.5	2.9	0.0418	12.9	13.0	0.9
0.0311	28.8	30.1	4.4	0.0517	15.3	15.9	3.7	0.0628	11.2	11.5	2.3
0.0415	24.9	26.0	4.2	0.0689	13.4	14.0	4.3	0.0837	9.9	10.2	3.4

$\varepsilon=1.5$				$\varepsilon=0.9$				$\varepsilon=0.8$			
Kn	$f Re_{\sqrt{A}}$ [19]	$f Re_{\sqrt{A}}$ (model)	Error (%)	Kn	$f Re_{\sqrt{A}}$ [19]	$f Re_{\sqrt{A}}$ (model)	Error (%)	Kn	$f Re_{\sqrt{A}}$ [19]	$f Re_{\sqrt{A}}$ (model)	Error (%)
0.0000	15.4	14.5	6.1	0.0000	15.3	13.7	11.5	0.0000	15.4	13.7	12.7
0.0009	15.3	14.4	5.9	0.0009	15.2	13.7	11.3	0.0009	15.3	13.6	12.5
0.0045	14.8	14.0	5.4	0.0045	14.7	13.3	10.6	0.0044	14.8	13.3	11.7
0.0067	14.5	13.8	5.0	0.0067	14.5	13.1	10.1	0.0066	14.5	13.1	11.2
0.0090	14.3	13.6	4.7	0.0089	14.2	12.9	9.7	0.0088	14.3	12.9	10.7
0.0225	12.8	12.5	3.0	0.0223	12.8	11.9	7.4	0.0221	12.8	11.9	8.2
0.0449	11.0	10.9	0.8	0.0447	11.0	10.5	4.5	0.0442	11.0	10.5	4.9
0.0674	9.7	9.7	0.9	0.0670	9.6	9.4	2.2	0.0663	9.6	9.4	2.5
0.0899	8.6	8.8	2.2	0.0894	8.6	8.5	0.5	0.0884	8.6	8.5	0.6

$$\text{Error} = \frac{f Re_{\sqrt{A}} [19] - f Re_{\sqrt{A}} [\text{model}]}{f Re_{\sqrt{A}} [\text{model}]} \times 100$$

$$\sin \alpha = \frac{1}{\sqrt{\varepsilon^2 - \beta \varepsilon^2 + 1}} \quad (25)$$

Bahrami et al. [22] presented the Poiseuille number for the no-slip condition as

$$f Re_{\sqrt{A}}^{\text{no-slip}} = \frac{4\pi^2[(3\varepsilon^2 + 1) + \beta(-3\varepsilon^2 + 1)]\varepsilon\sqrt{\varepsilon}}{9(\varepsilon + \sqrt{\varepsilon^2 - \beta \varepsilon^2 + 1})} \quad (26)$$

Using Eqs. (16) and (26) one can calculate  $f Re_{\sqrt{A}}$ . In Table 5 the predicted results of the proposed model are compared with the numerical data of Morini et al. [19] with  $\alpha=54.74$  deg. The agreement between the present model and the numerical data is within 8%; however, there are a few points, especially at relatively high or low aspect ratios, where differences up to 12% are observed.

Figure 4 shows the comparison between the proposed model and the experimental data of Araki et al. [18] for trapezoidal microchannels with  $\alpha=54.74$  deg. They used two different channels with dimensions  $b=41.5 \mu\text{m}$  and  $41.2 \mu\text{m}$  and  $h=5.56 \mu\text{m}$  and  $2.09 \mu\text{m}$ , respectively. These channels were made of silicon wafer with hydraulic diameters of  $9.41 \mu\text{m}$  and  $3.92 \mu\text{m}$ . They conducted tests with nitrogen and helium over a range of  $0.011 < Kn < 0.035$  and  $0.05 < Re < 4.2$ . The uncertainty of their measurements was reported to be 10.9%. As shown in Fig. 4, the values predicted by the model are within 10% accuracy of the data.

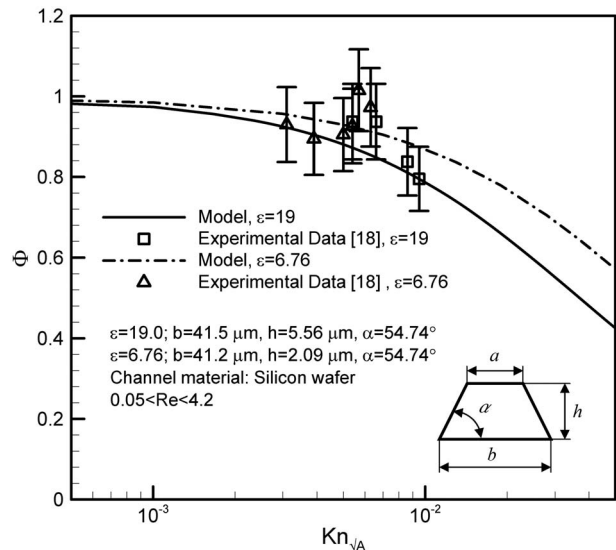
**5.4 Double-Trapezoidal Microchannels.** Double-trapezoidal cross section geometry is depicted in Table 1. Same as the trapezoidal cross section, the nondimensional parameter  $\beta$  is defined by Eq. (24).

Table 6 and Fig. 5 present the comparison between the proposed model with numerical data of Morini et al. [19] for  $\alpha$

$=54.74$  deg. As can be seen, except for a few points, the agreement between the model and the numerical values is less than 8%.

## 6 Summary and Conclusions

Pressure drop of the fully-developed, incompressible slip-flow through microchannels of general cross sections is investigated. An averaged first-order Maxwell boundary condition is assumed



**Fig. 4 Comparison of the model with experimental data of Araki et al. [18] for trapezoidal channels ( $\alpha=54.74$  deg)**

**Table 6 Model versus data [19]; double-trapezoidal channels**

$\varepsilon=0.83$				$\varepsilon=0.96$				$\varepsilon=1.29$			
Kn	$f Re_{\sqrt{A}}$ [19]	$f Re_{\sqrt{A}}$ (model)	Error (%)	Kn	$f Re_{\sqrt{A}}$ [19]	$f Re_{\sqrt{A}}$ (model)	Error (%)	Kn	$f Re_{\sqrt{A}}$ [19]	$f Re_{\sqrt{A}}$ (model)	Error (%)
0.0000	14.8	13.8	6.6	0.0000	14.7	13.9	6.0	0.0000	14.3	13.7	4.2
0.0010	14.6	13.7	6.5	0.0010	14.6	13.8	5.9	0.0011	14.1	13.6	4.1
0.0050	14.2	13.4	6.1	0.0051	14.1	13.4	5.5	0.0053	13.7	13.2	3.8
0.0075	13.9	13.2	5.8	0.0077	13.9	13.2	5.3	0.0079	13.5	13.0	3.7
0.0100	13.7	12.9	5.5	0.0103	13.6	13.0	5.1	0.0106	13.2	12.8	3.5
0.0251	12.3	11.8	4.2	0.0256	12.3	11.8	4.0	0.0265	11.9	11.6	2.8
0.0501	10.5	10.3	2.5	0.0513	10.5	10.2	2.6	0.0530	10.2	10.0	1.8
0.0752	9.2	9.1	1.2	0.0769	9.2	9.0	1.5	0.0795	9.0	8.9	1.0
0.1002	8.2	8.2	0.2	0.1025	8.2	8.1	0.7	0.1060	8.0	7.9	0.4

$\varepsilon=1.515$				$\varepsilon=1.79$				$\varepsilon=2.63$			
Kn	$f Re_{\sqrt{A}}$ [19]	$f Re_{\sqrt{A}}$ (model)	Error (%)	Kn	$f Re_{\sqrt{A}}$ [19]	$f Re_{\sqrt{A}}$ (model)	Error (%)	Kn	$f Re_{\sqrt{A}}$ [19]	$f Re_{\sqrt{A}}$ (model)	Error (%)
0.0000	14.1	13.6	3.5	0.0000	14.0	13.6	3.0	0.0000	14.7	14.3	2.9
0.0011	14.0	13.5	3.4	0.0011	13.9	13.5	3.0	0.0010	14.6	14.2	2.8
0.0053	13.5	13.1	3.2	0.0054	13.5	13.1	2.8	0.0052	14.1	13.8	2.6
0.0080	13.3	12.9	3.0	0.0080	13.2	12.9	2.6	0.0079	13.8	13.5	2.5
0.0107	13.1	12.7	2.9	0.0107	13.0	12.7	2.5	0.0105	13.6	13.3	2.4
0.0267	11.8	11.5	2.2	0.0268	11.7	11.5	1.9	0.0262	12.2	12.0	1.7
0.0534	10.1	10.0	1.3	0.0536	10.1	10.0	1.0	0.0525	10.5	10.4	0.9
0.0802	8.9	8.8	0.7	0.0803	8.8	8.8	0.4	0.0787	9.2	9.1	0.3
0.1069	7.9	7.9	0.2	0.1071	7.9	7.9	0.1	0.1049	8.1	8.2	0.2

$$\text{Error} = \frac{f Re_{\sqrt{A}} [19] - f Re_{\sqrt{A}} [\text{model}]}{f Re_{\sqrt{A}} [\text{model}]} \times 100$$

on the channel walls. Introducing a relative velocity, axial momentum equation reduces to Poisson's equation with no-slip boundary condition. Following Bahrami et al. [22,23] and using analytical solution for elliptical microchannels, a compact model is developed that predicts the Poiseuille number as a function of geometrical parameters of the duct. The presented model is more general than the model of Bahrami et al. and covers both slip-flow and no-slip regimes.

The model is successfully validated against existing numerical and experimental data in literature for a variety of shapes including circular, rectangular, trapezoidal, and double-trapezoidal cross sections, with a relative difference on the order of 8%.

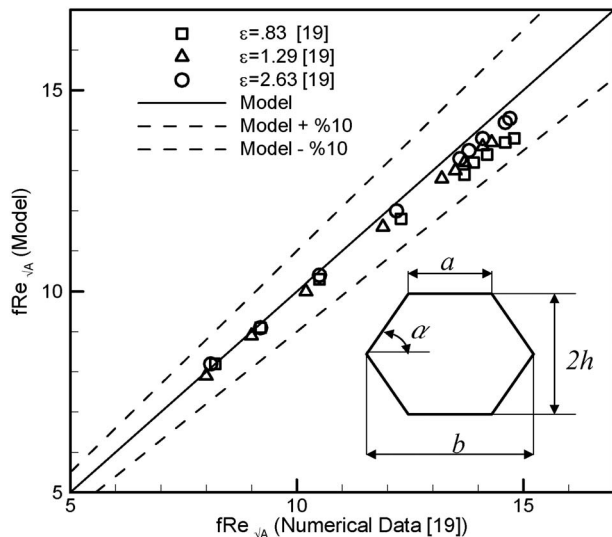
Employing the proposed model, one only needs to compute the nondimensional parameter  $I_p^* \sqrt{A} / \Gamma$  of the channel to determine the Poiseuille number. On the other hand, using the conventional method, Poisson's equation must be solved with slip boundary condition to find the velocity field and the mean velocity often numerically. Then the averaged wall shear stress should be calculated to find  $f Re_{\sqrt{A}}$ . This clearly shows the convenience of the proposed approximate model.

**Acknowledgment**

The authors gratefully acknowledge the financial support of the Natural Sciences and Engineering Research Council of Canada (NSERC).

**Nomenclature**

- $A$  = cross sectional area,  $m^2$
- $C$  = sound velocity,  $m/s$
- $D_h$  = hydraulic diameter,  $m$
- $E(\cdot)$  = complete elliptic integral of the second kind
- $f Re$  = Poiseuille number
- $I_p$  = polar moment of inertia,  $m^4$
- $I_p^*$  = dimensionless polar moment of inertia,  $I_p/A^2$
- Kn = Knudsen number
- $\mathcal{L}$  = characteristic length,  $m$
- Ma = Mach number,  $Ma = u/C$
- $P$  = pressure,  $N/m^2$
- Re = Reynolds number
- $\sqrt{A}$  = square root of area,  $m$



**Fig. 5 Comparison of the model with numerical data of Morini et al. [19] for double-trapezoidal conduits**

$u$  = axial velocity, m/s  
 $u_s$  = local slip-velocity, m/s  
 $\bar{u}_s$  = average slip-velocity, m/s  
 $U$  = relative velocity, m/s

### Greek Symbols

$\Gamma$  = perimeter, m  
 $\varepsilon$  = aspect ratio  
 $\lambda$  = molecular mean free path, m  
 $\mu$  = viscosity, N s/m<sup>2</sup>  
 $\sigma$  = tangential momentum accommodation factor  
 $\bar{\tau}_w$  = averaged wall shear stress, N/m<sup>2</sup>  
 $\tau_w$  = local shear stress, N/m<sup>2</sup>  
 $\Phi$  = reduction in friction coefficient in slip condition,  $f \text{ Re}_{\sqrt{A}}/f \text{ Re}_{\sqrt{A}}^{\text{no-slip}}$

### References

- [1] Tuckerman, D. B., and Pease, R. F., 1981, "High-Performance Heat Sinking for VLSI," *IEEE Electron Device Lett.*, **2**, pp. 126–129.
- [2] Hsieh, S. S., Tsai, H. H., Lin, C. Y., Huang, C. F., and Chien, C. M., 2004, "Gas Flow in a Long Microchannel," *Int. J. Heat Mass Transfer*, **47**, pp. 3877–3887.
- [3] Zhu, X., Liao, Q., and Xin, M. D., 2006, "Gas Flow in Microchannel of Arbitrary Shape in Slip Flow Regime," *Microscale Thermophys. Eng.*, **10**(1), pp. 41–54.
- [4] Kim, M. S., Araki, T., Inaoka, K., and Suzuki, K., 2000, "Gas Flow Characteristics in Microtubes," *JSME Int. J., Ser. B*, **43**(4), pp. 634–639.
- [5] Bahrami, M., Yovanovich, M. M., and Culham, J. R., 2006, "Pressure Drop of Fully-Developed, Laminar Flow in Rough Microtubes," *ASME J. Fluids Eng.*, **128**, pp. 632–637.
- [6] Morini, G. L., 2004, "Laminar-to-Turbulent Flow Transition in Microchannels," *Microscale Thermophys. Eng.*, **8**, pp. 15–30.
- [7] Wu, H. Y., and Cheng, P., 2003, "Friction Factors in Smooth Trapezoidal Silicon Microchannels With Different Aspect Ratios," *Int. J. Heat Mass Transfer*, **46**, pp. 2519–2525.
- [8] Renksizbulut, M., Niazmand, H., and Tercan, G., 2006, "Slip Flow and Heat Transfer in Rectangular Microchannels With Constant Wall Temperature," *Int. J. Therm. Sci.*, **45**, pp. 870–881.
- [9] Pfahler, J., Harley, J., Bau, H., and Zemel, J. N., 1991, "Gas and Liquid Transport in Small Channels," *Micromechanical Sensors, and Actuators Systems*, ASME DSC 32, Winter Annual Meeting, Atlanta, GA, pp. 49–58.
- [10] Ebert, W. A., and Sparrow, E. M., 1965, "Slip Flow in Rectangular and Annular Ducts," *ASME J. Basic Eng.*, **87**, pp. 1018–1024.
- [11] Harley, J., Huang, Y., Bau, H., and Zemel, J. N., 1995, "Gas Flow in Microchannels," *J. Fluid Mech.*, **284**, pp. 257–274.
- [12] Morini, G. L., and Spiga, M., 1998, "Slip Flow in Rectangular Microtubes," *Microscale Thermophys. Eng.*, **2**(4), pp. 273–282.
- [13] Beskok, A., and Karniadakis, G. E., 1999, "A Model for Flows in Channels, Pipes, and Ducts at Micro and Nano Scales," *Microscale Thermophys. Eng.*, **3**, pp. 43–77.
- [14] Choi, S. B., Barron, R. F., and Warrington, R. O., 1991, "Fluid Flow and Heat Transfer in Microtubes," *Micromechanical Sensors, Actuators, and Systems*, ASME DSC 32, Winter Annual Meeting, Atlanta, GA, pp. 123–134.
- [15] Yu, D., Warrington, R., Barron, R., and Ameen, T., 1995, "An Experimental and Theoretical Investigation of Fluid Flow and Heat Transfer in Microtubes," *ASME/JSME Thermal Engineering Conference*, Vol. 1, pp. 523–530.
- [16] Arkilic, E. B., Schmidt, M. A., and Breuer, K. S., 1997, "Gaseous Slip Flow in Long Microchannels," *J. Microelectromech. Syst.*, **6**(2), pp. 167–178.
- [17] Arkilic, E. B., Breuer, K. S., and Schmidt, M. A., 2001, "Mass Flow and Tangential Momentum Accommodation in Silicon Micromachined Channels," *J. Fluid Mech.*, **437**, pp. 29–43.
- [18] Araki, T., Kim, M. S., Hiroshi, I., and Suzuki, K., 2000, "An Experimental Investigation of Gaseous Flow Characteristics in Microchannels," *Proceedings of International Conference on Heat Transfer and Transport Phenomena in Microscale*, Begell House, New York, pp. 155–161.
- [19] Morini, G. L., Spiga, M., and Tartarini, P., 2004, "The Rarefaction Effect on the Friction Factor of Gas Flow in Micro/Nano-Channels," *Superlattices Microstruct.*, **35**(3–6), pp. 587–599.
- [20] Khan, W. A., and Yovanovich, M. M., 2007, "Analytical Modeling of Fluid Flow and Heat Transfer in Micro/Nano-Channel Heat Sinks," *Proceedings of the IPACK2007*, Vancouver, BC, Canada.
- [21] Duan, Z., and Muzychka, Y. S., 2007, "Slip Flow in Non-Circular Microchannels," *Microfluid. Nanofluid.*, **3**, pp. 473–484.
- [22] Bahrami, M., Yovanovich, M. M., and Culham, J. R., 2006, "Pressure Drop of Laminar, Fully Developed Flow in Microchannels of Arbitrary Cross Section," *ASME J. Fluids Eng.*, **128**, pp. 1036–1044.
- [23] Bahrami, M., Yovanovich, M. M., and Culham, J. R., 2007, "A Novel Solution for Pressure Drop in Singly Connected Microchannels of Arbitrary Cross Section," *Int. J. Heat Mass Transfer*, **50**, pp. 2492–2502.
- [24] White, F. M., 1984, *Viscous Fluid Flow*, McGraw-Hill, New York.
- [25] Roy, S., Raju, R., Chuang, H. F., Cruden, B. A., and Meyyappan, M., 2003, "Modeling Gas Flow Through Microchannels and Nanopores," *J. Appl. Phys.*, **93**(8), pp. 4870–4879.
- [26] Karniadakis, G. E., and Beskok, A., 2002, *Micro Flows: Fundamentals and Simulation*, Springer, New York.
- [27] Yovanovich, M. M., 1974, "A General Expression for Predicting Conduction Shape Factors," *AIAA, Thermophysics and Space Craft Control*, Cambridge, Mass. London: MIT Press, 35, pp. 265–291.
- [28] Yovanovich, M. M., 1987, "New Nusselt and Sherwood Numbers for Arbitrary Isopotential Bodies at Near Zero Peclet and Rayleigh Numbers," *AIAA 22nd Thermophysics Conference*, Honolulu, HI.
- [29] Muzychka, Y. S., and Yovanovich, M. M., 2002, Laminar Flow Friction and Heat Transfer in Non-Circular Ducts and Channels Part, 1: *Hydrodynamic Problem*, *Compact Heat Exchangers: A Festschrift on the 60th Birthday of Ramesh K. Shah*, Grenoble, France, pp. 123–130.
- [30] Bejan, A., 1995, *Convection Heat Transfer*, Wiley, Englewood Cliffs, NJ.
- [31] Morini, G. L., Lorenzini, M., and Spiga, M., 2005, "A Criterion for Experimental Validation of Slip-Flow Models for Incompressible Rarefied Gases Through Microchannels," *Microfluid. Nanofluid.*, **1**, pp. 190–196.